Nour et al.
Protection and Control of Modern Power Systems (2023) 8:20
https://doi.org/10.1186/s41601-023-00293-y

Protection and Control of
Modern Power Systems

ORIGINAL RESEARCH

Open Access

Voltage imbalance mitigation in an active distribution network using decentralized current control

Ahmed M. M. Nour[1*], Ahmed A. Helal[2], Magdi M. El-Saadawi[3] and Ahmed Y. Hatata[3,4]

Abstract

Voltage imbalance (VI) is caused by the difference in connected single-phase load or generation in a low voltage distribution network (DN).VI increase in a smart distribution grid is due to the current practice of increasing single-phase distributed generators such as photovoltaic (PV) systems. This paper proposes a decentralized control method to mitigate VI using distributed batteries included in smart grid interfaced residential PV systems. To mitigate VI using the batteries in this way, five challenges must be overcome, i.e., equalizing all battery stress currents within the DN, mitigating VI in abnormal conditions such as signal loss among bus controllers, being immune from the distorted feedback measurements, minimizing the steady-state error at different loads, and overcoming the insufficient number or capacity of the distributed batteries at the same bus. Three fuzzy logic controllers (FLC) are proposed at each bus to overcome these five tasks based on a decentralized control scheme. The proposed decentralized control based on FLC is compared with centralized control based on a PI controller. The proposed control method is tested and verified using simulations in the MATLAB/Simulink software, and the results validate the ability of the scheme to alleviate VI on a smart distribution network under both normal and abnormal conditions.

Keywords Fuzzy controller, Distributed batteries, Decentralized control, Voltage imbalance, Distributed PV

1 Introduction

Distributed generators (DGs), especially single-phase PV systems, have been widely installed in low-voltage smart grids. Consequently, the non-symmetry of the power flow among the three phases in the distribution network (DN) causes high voltage imbalance (VI) and high overvoltage problems. Unbalanced DN is exposed to higher overvoltage and neutral current than a balanced DN, while high VI causes many problems, such as high line power losses, instability, and high neutral voltage. These affect the sensitive loads in the DN [1–3]. Also, the ability to carry the load of the DN decreases with the increase in unbalanced PVs and/or loads [4]. Therefore, suppressing VI can reduce many negative impacts on the DN. Several strategies have been used to decrease VI in DN, such as re-phasing loads, on-load tap changer (OLTC) and Demand Response (DR), active power curtailment (APC), reactive power, and energy storage systems [5–17].

In the re-phasing load strategy, the loads are transferred from the overloaded phases to other phases by calculating the different power and/or current. VI along the DN can be minimized using an optimization method such as bacterial foraging [5], while smart meters can provide the necessary measurements. The studied control system

*Correspondence:
Ahmed M. M. Nour
ahmed.nour@aiet.edu.eg
[1] Alexandria Higher Institute of Engineering and Technology (AIET), Alexandria, Egypt
[2] Department of Electrical and Control Engineering, Arab Academy for Science and Technology and Maritime Transport, Alexandria, Egypt
[3] Department of Electrical Engineering, Faculty of Engineering, Mansoura University, Mansoura, Egypt
[4] Department of Electrical Engineering, College of Engineering, Shaqra University, Shaqra, Kingdom of Saudi Arabia

boosts the hosting capacity of the DN and suppresses VI to be less than 1%. In this method, the installation cost of the re- phasing switches is relatively small in comparison to the reconfiguration of the DN. In [6], a modified particle swarm optimization algorithm controls the independent OLTC and DR to mitigate both overvoltage and VI. The optima of both switched residential loads and OLTC taps are determined. Although this strategy is effective, it requires large communication signals. In addition, both strategies in [5, 6] are vulnerable to communication failure and distorted signals.

A modified droop control method mitigates both overvoltage and VI based on voltage droop and a damping control strategy. This method depends on local measurements only and requires lower inverter capacities than conventional droop control systems [7]. A two-level control strategy is proposed in [8] based on a centralized control scheme. The first level mitigates both overvoltage and VI based on the droop curve and damping conductance matrix, while the second level is an overlay control consisting of OLTC control and fair power-sharing to minimize the overall APC and to appropriately re-share the curtailed power based on the location of the DG.

A coordinating method for reactive power from PV inverter, OLTC, and shunt capacitor switching is introduced in [9]. The control method minimizes the tapping in both OLTC and capacitor switches by using an enhanced genetic algorithm on the Fuzzy Logic Controller (FLC). The results showed that both power loss and VI are reduced, although VI values are different along the DN, resulting in some PV inverters injecting more reactive power than others.

Many control strategies have recently been developed based on energy storage systems (ESS) [10–17]. Reference [10] uses groups of ESS in different zone areas to regulate node voltages in DN with PV plants. After determining the valid ESSs, the ESS groups inject active power based on both the voltage sensitivity matrix and the ESS zone area. The studied system is tested on the IEEE 33-bus medium voltage DN. In [11], batteries in rooftop PV systems are exploited to suppress overvoltage in the DN. With restricted communication links, both the local and distributed control schemes coordinate the required power at the suitable time and coping with the shortage of battery capacities. However, in [10, 11], the validity of both control systems under unbalanced DN is not checked.

A smart charging control method for Electric Vehicles (EV) is presented in [12]. An optimization method is used to minimize two objective functions: charging cost and load variance in the DN. Fuzzy control is applied to minimize either load variance or heavy load. In [13], EVs minimize VI in the DN, but despite promising results, the control method is complex because of high communication requirements in the coordinated control. Reference [14] uses day-ahead scheduling active and reactive power in the microgrid to fulfil multi-objective functions such as minimizing VI, line power loss, peak shaving, energy cost, and voltage deviations, while maximizing the security margin.

In [15], a particle swarm optimization technique manages the energy storage in the unbalanced DN to perform four objective functions: VI, voltage deviation, power curtailment, and line power loss. The results show that residential storage is the most efficient in alleviating both VI and voltage deviation. However, the VI value is close to 0% rather than the standard limit value, and thus it causes over-stress on batteries.

In [16], distributed battery inverters in the phases are controlled to suppress VI by FLC. Based on the state of charge (SoC) status and phase voltage values, a phase selector guides the FLC to compute reference current of the battery inverter at a certain phase. However, the control system does not apply in the multi-bus network. In [17], VI is mitigated in the DN by using two PI controllers, whose outputs are the ratio of the battery currents for VI mitigation and the unified value of battery stresses along the DN. In addition, there is an optimization algorithm to determine the battery shares based on the SoC of the batteries at the same bus. However, this system requires complex calculations and many communication links. In addition, it is not immune to the loss of signals and noises accompanying the measurement signals. Both systems of [16, 17] are of a central control scheme type so any failure in the communication link can cause maloperation of the whole system.

The deficiencies in [17] are the many communication links in the control system. These make it impossible in large DN to solve noise and loss in the feedback signals. It is difficult to tune PI-controllers' parameters in large DN, and there is high computation cost in determining the optimal stress on each battery at the same bus. This paper proposes a control system that avoids the above weaknesses.

The main contribution of this paper is to mitigate VI in the three-phase four-wire radial DN with distributed PV systems using batteries. The proposed control system, based on three FLCs, is used to solve the following five challenges:

– Equalizing all battery stress currents in the DN. As the last bus is prone to high VI in comparison to others, so the batteries at the last bus inject the highest currents while batteries at the first bus inject low currents.

- Avoiding the impact of temporary signal loss among buses, loss which can lead to system failure.
- Solving the insufficient capacity problem of the distributed batteries at the same bus.
- Avoiding the impact of noise in the feedback measurements.
- Minimizing the steady-state error at different load values.

The rest of the paper is organized as follows. Section 2 explores the control system in the DN, while in Sect. 3, the control scheme based on a decentralized system is proposed. Section 4 describes the system and Sect. 5 illustrates the results and discussions. The conclusion is presented in Sect. 6.

2 Control system scheme of DN

A communication system is essential in a smart grid to transmit signals among controllers. There is no standard form for the communication/network frame in a smart grid and each smart grid has its own communication strategy [18]. There are two types of communication methods: wired and wireless. The wired method is the most secure and reliable [19, 20], while wireless techniques have advantages in both cost and for future expansion [21].

2.1 The applied control scheme types in the smart grid

In a smart grid, the control system can be classified into local, centralized, decentralized, and distributed control schemes. The local controller is dedicated to a certain small system while neglecting the interaction with the others, such as the end-user controller in a residential PV system. The centralized control scheme depends on a main controller for the whole network, so this system is prone to collapse because of long communication delays, failures in communication links, and high computational burden. In contrast, the decentralized control scheme depends on each grid's subsystem controller communicating with its neighbors, whereas in the distributed control scheme, both the subsystem controller and local controller of the grid communicate with their neighbors [19, 22].

The control scheme is supported by three communication tiers: Home Area Networks (HAN), Neighborhood Area Networks (NAN), and Wide Area Networks (WAN) [23]. Distributed generators, loads, and battery systems communicate through HAN in residential loads. In the case of NAN, smart meters can communicate with the central controller to provide their measurements such as voltages, currents, and SOC of batteries. The controllers send their data to the utility operators through WAN.

2.2 Internet of Things (IoT) in smart grid

HAN, WAN, and NAN may not be required in a smart grid which is applying IoT. IoT is internet-connected devices where sensors and actuators are interacting with each other. It allows the control and monitoring of numerous things in the smart grid, so IoT is the best choice to deal with a huge amount of data in the smart grid [24]. Both smart inverters and smart meters can be connected through the internet and controlled by IoT, and thus, they can be exploited to perform several functions in a smart grid such as consumer energy efficiency, smart grid management, and power quality improvement [25]. Reference [26] presents a smart meter connected to the IoT with a harmonic analyzer. For accurate measurement, voltage, current, and power must be identified and then sent without harmonic distortion to the cloud. Based on accurate data, energy management in the smart grid is enhanced. Also, the IoT is the best option for sending a huge amount of collected measurement data for optimum energy management [27]. However, the IoT is still underdeveloped in the smart grid. In 2019, the percentages using IoT in smart homes and smart utility sectors are only 14% and 4%, respectively.

2.3 Proposed control scheme

We adopt the decentralized control system because of its small number of communication links. Consequently, fewer errors are possible among controllers.

The last bus may violate the VI limit while other buses are within the VI limits, so battery systems at the last bus have the highest stress [28]. To ensure all buses operate together and share the same stress based on the last bus, two types of reference signals of decentralized control systems are investigated, i.e., cascade and common. The first scheme is based on each bus following its neighbor as presented in Fig. 1a. For the second scheme, it requests all buses to follow the leader bus as presented in Fig. 1b, in which the leader controller is implemented on the bus prone to the highest VI while the other buses are controlled by the follower controllers.

VI violation has long duration, and thus, high data rate is not a merit in this application [29]. The selection of communication technology is beyond the scope of this paper.

3 Proposed control scheme based on the decentralized scheme

The proposed control scheme consists of bus controllers that receive the measurements from the smart meters in each house. Smart meters have the ability to measure both consumers' voltages and currents, and communicate with other devices [30, 31]. Therefore, they can be

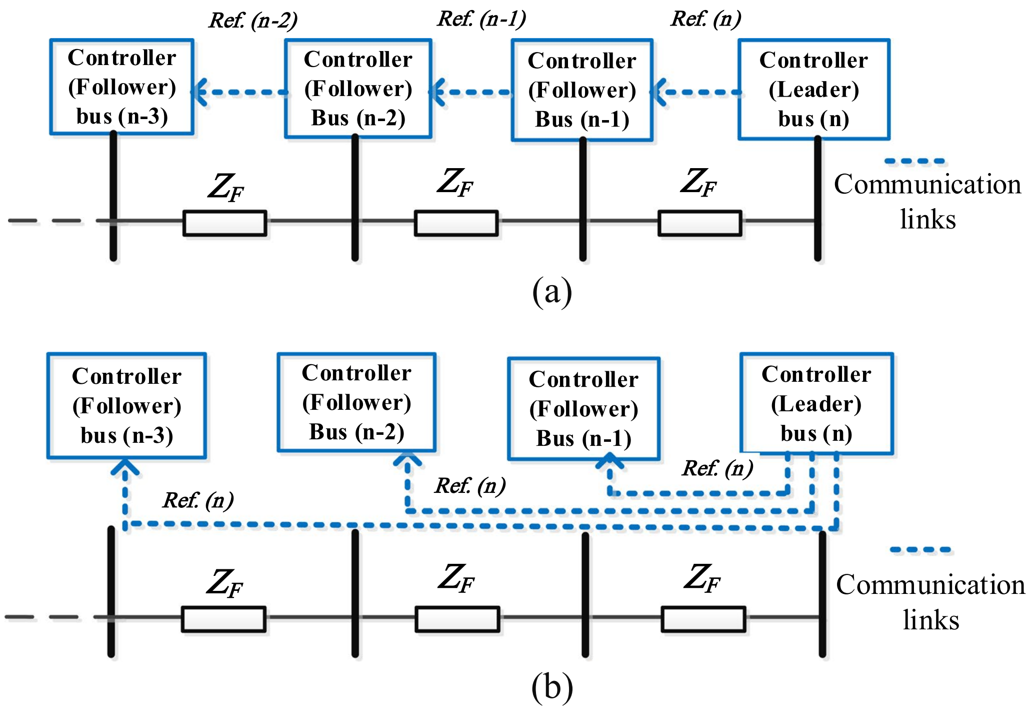

Fig.1 Reference's signal type; **a** cascaded, **b** common

exploited to suppress voltage violations in the smart grid. Figure 2 illustrates the bus control scheme at the *j*th bus. Each house in the distribution system involves a PV generation unit, load consumption, and battery system. The integrated battery with the PV system has bidirectional power flow to fulfill self-consumption. As well as the main function of the battery system, the bus controller can manage the injected battery current to mitigate VI in the case of high VI value.

The output of the controller is the ratio of the compensating battery current at each bus. Unlike a PI controller, FLC has high effectiveness in dealing with imperfect signals and requires fewer communication links [32]. In addition, FLC has an extra degree of flexibility in comparison with the conventional PI controller, and it deals effectively with muti-inputs/outputs and nonlinear systems [33]. Therefore, FLCs are the backbone of this paper.

In the proposed controller, the bus controller consists of three FLCs to mitigate VI, guarantee the same stress as other buses, and consider the SoC status of batteries in each phase. Figure 3 presents the schematic block diagram of the bus controllers at the *j*th bus.

FLC (1) is used to mitigate VI at the *j*th bus and its output is the ratio of the bus compensating currents. FLC (2) is used to ensure all buses share the same value of the battery stress current, and FLC (3) is for re-sharing the stress on batteries at the same bus at different phases based on their SoC status. The output of the bus controller is the battery stress current of each phase. Each bus controller will be discussed in detail in the following subsections.

Based on the EN 50,160 standard, VI must not exceed 2% [29]. To ensure compliance, the phase reference currents of the AC coupling battery systems at the *j*th bus are expressed by:

$$I_{ref,a,j} = \lambda_{a,j} \times \delta_j \times I_{n,j} \tag{1}$$

$$I_{ref,b,j} = \lambda_{b,j} \times \delta_j \times I_{n,j} \tag{2}$$

$$I_{ref,c,j} = \lambda_{c,j} \times \delta_j \times I_{n,j} \tag{3}$$

where $I_{ref,a,j}$, $I_{ref,b,j}$ and $I_{ref,c,j}$ are the battery reference currents for phases *a*, *b*, and *c*, respectively. δ_j is the required ratio of bus compensating battery currents at the *j*th bus for mitigating VI. $\lambda_{a,j}$, $\lambda_{b,j}$, and $\lambda_{c,j}$ are the respective sharing coefficients at the *j*th bus for phases *a*, *b*, and *c* for distributing battery currents based on the SoC status of each battery. $I_{n,j}$ is the injected neutral current percentage at the *j*th bus.

3.1 First controller FLC (1)

FLC (1) determines the required ratio of battery phase reference currents δ_j at the *j*th bus for implementing two functions: mitigating VI at the buses and ensuring the same stress currents among all buses. FLC (1) is designed

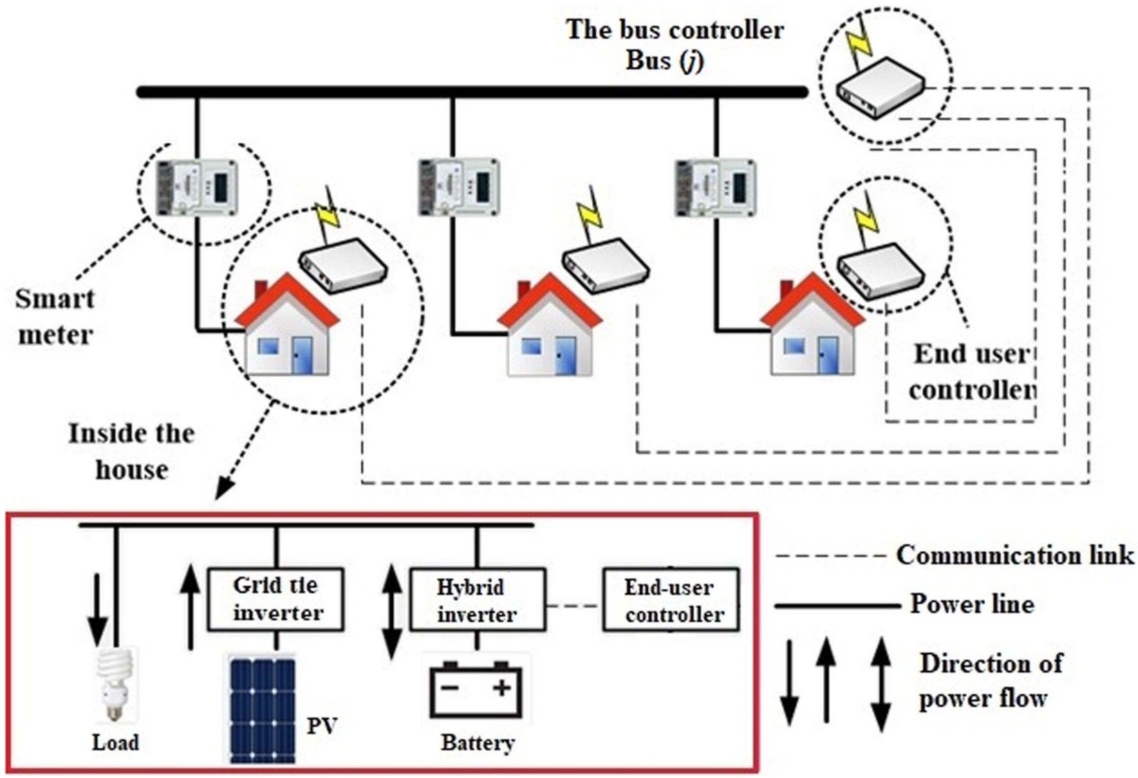

Fig. 2 The control scheme at any *j*th bus

to operate as a PI controller, and there are two types of FLC (1), i.e., FLC (*1-Leader*) on the leader bus and FLC (*1-Follower*) on the rest of the DN buses. They depend on Mamdani fuzzy inference systems and the defuzzification method is the centroid.

3.1.1 FLC (1-Leader)

FLC (*1-Leader*) is applied at the last bus in the radial DN because its VI has the highest value. As presented in Fig. 4, FLC (*1-Leader*) has two inputs, i.e., the error *e(k)* and the change of error *Δe(k)* at the sample *k*, and one output of δ(*k*) at the sample *k*. The output of FLC (*1-Leader*) is the ratio of the compensating battery currents δ_j at the last bus in the DN for restricting VI according to the EN 50,160 standard limit. The FLC (1) input *e(k)* is the difference between the measured and reference VI values, i.e.:

$$e(k) = VU_{meas.,j}(k) - VU_{ref.}(k) \tag{4}$$

The limiter before the VI_{ref} block is to ensure that the FLC (1) input becomes zero when $VI_{meas,j}$ is below the standard as depicted in Fig. 3. The discrete output of the FLC, $\Delta\delta$, is the rate change of the ratio of bus compensating battery currents and can be expressed as:

$$\Delta\delta(k) = K_P \Delta e(k) + K_I e(k) \tag{5}$$

where $\Delta e(k)$ is the rate of change of difference VI at interval *k*. K_P and K_I are the proportional and integral gains, respectively. The ratio of bus compensating battery currents is the summation of the previous sample value and the rate of change of the output, i.e.:

$$\delta(k) = \Delta\delta(k) + \delta(k-1) \tag{6}$$

Figure 5 illustrates five input and five output membership functions of FLC (1- *Leader*) while the rules of FLC (1-*Leader*) are illustrated in Table 3 in the Appendix.

3.1.2 FLC (1-Follower)

VI at the feeder end is much larger than that at the feeder beginning. Consequently, the batteries on the bus with the highest VI inject high current values in comparison to their counterparts on other buses. Therefore, it is necessary to guarantee that all batteries on all buses have the same compensating currents. FLC (1-follower) is designed and applied in the rest of the buses for this purpose. They operate like FLC (1- *Leader*) and the output is the ratio of the battery compensating currents for mitigating VI at the *j*th bus. The batteries' current stress $I_{stress,j}$ at the *j*th bus can be expressed by [17]:

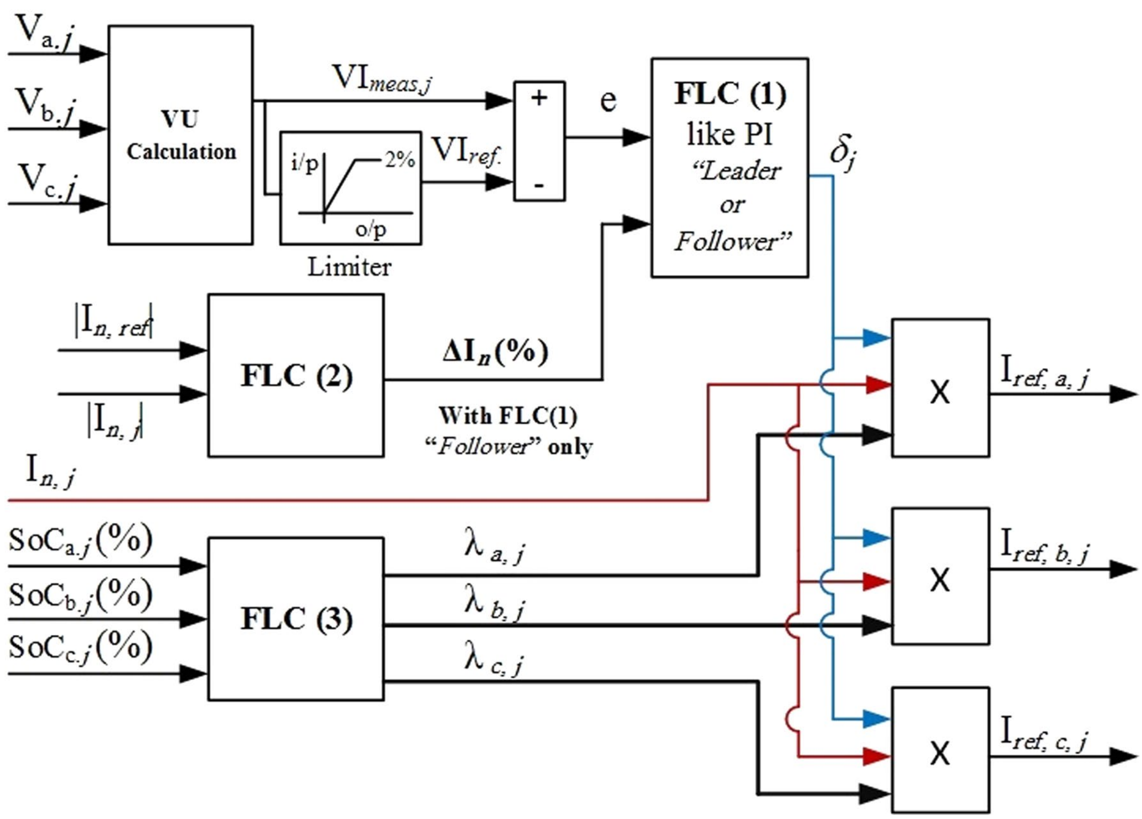

Fig. 3 Schematic block diagram of the bus controller at the *j*th bus

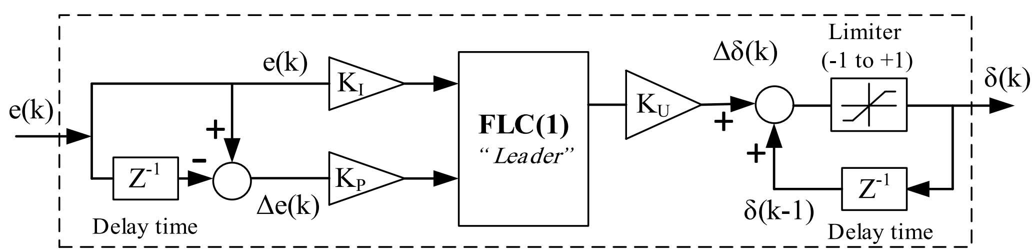

Fig. 4 Schematic block diagram of FLC (1- *Leader*) for the leader bus

$$I_{stress,j} = \sqrt{\left(I_{ref,a,j}\right)^2 + \left(I_{ref,b,j}\right)^2 + \left(I_{ref,c,j}\right)^2} \quad (7)$$

The schematic block diagram of FLC (*1-Follower*) is shown in Fig. 6. It has three inputs: the error *e(k)*, the change of error Δ*e(k)*, and the change of battery current stress at the *j*th bus. The output is *δ(k)* at the interval *k*. The input and output membership functions of FLC (*1-Follower*) are presented in Fig. 7. The 5 input membership functions are: negative large (NL), negative small (NS), zero (Z), positive small (PS), and positive large (PL). There are 13 output membership functions designed for this controller.

Fuzzy sets {a, b, c, d, e, and f} are the negative value orders while Fuzzy sets {h, i, j, k, l, and m} are the positive value orders. The fuzzy set {g} is the zero-membership function as illustrated in Fig. 7. The rules of FLC (1-Follower) are presented in Table 4 in the Appendix, and the parameters of the FLC are presented in the DN in Table 4 in the Appendix.

3.2 Second controller FLC (2)

The third input of FLC (*1-Follower*) is the change of the stress currents needed to ensure the same battery stress current in all buses. It is the ratio of the difference

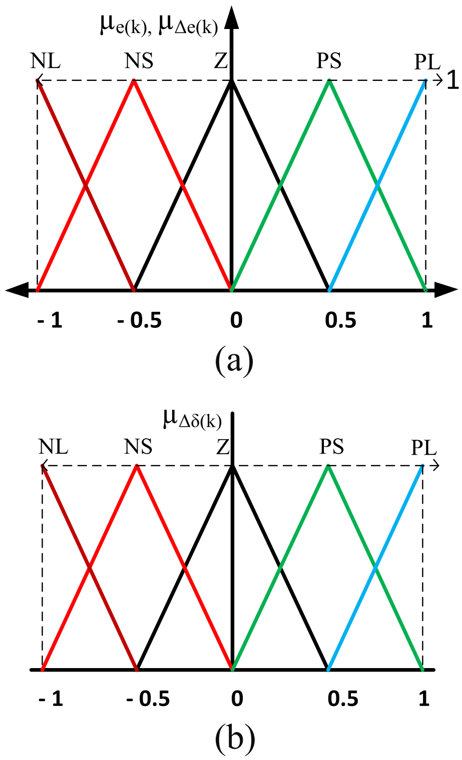

Fig. 5 Membership functions of FLC (1- *Leader*): **a** for the inputs; **b** for the outputs

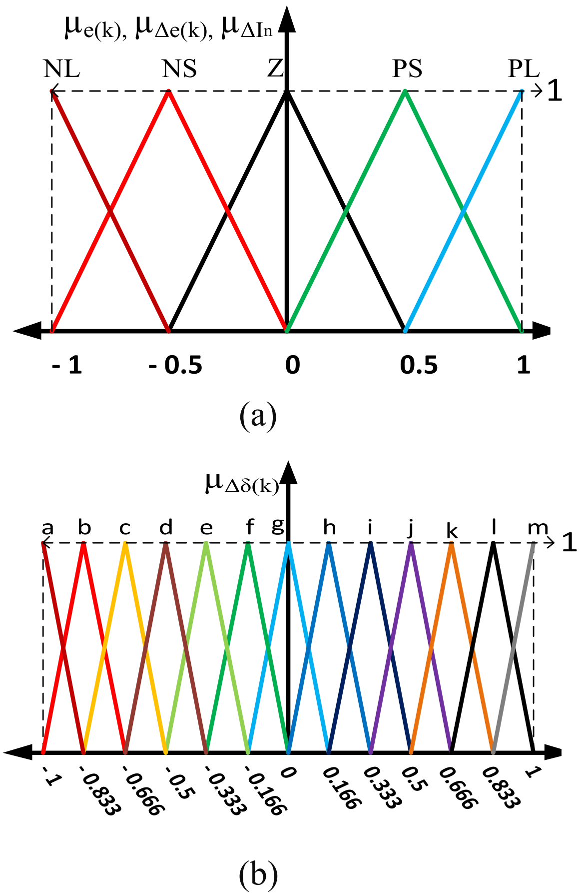

Fig. 7 Membership functions of FLC (1- *Follower*): **a** for the inputs; **b** for the outputs

between the reference and actual battery stress currents at the *j*th bus to the reference battery stress current as

$$\Delta I_{stress} = \frac{\left(I_{stress,ref} - I_{stress}\right)}{I_{stress,ref}} \tag{8}$$

However, in the case of signal loss, the reference stress current becomes zero and (8) becomes infinite. In that case, the FLC (1-follower) operates inappropriately, and therefore, FLC (2) is used instead. As presented in Fig. 3, the two inputs of FLC (2) are the reference battery stress current and battery stress current at any bus, while the output of FLC (2) is the change of the stress current. Figure 8 presents the input and output membership functions of FLC (2). As seen in Fig. 8a, b, there are 16 input membership functions and 13 output membership functions.

The first input function {A} has a very small value (ε) and represents the signal loss or no battery stress current is required. Based on the FLC (2) rules, if the reference battery stress current suddenly belongs to fuzzy set {A}, it refers to a signal loss so the battery stress current at any bus should keep its value until the signal is restored. Therefore, the output membership function is {Z}. However, there are two exceptions. The first exception occurs

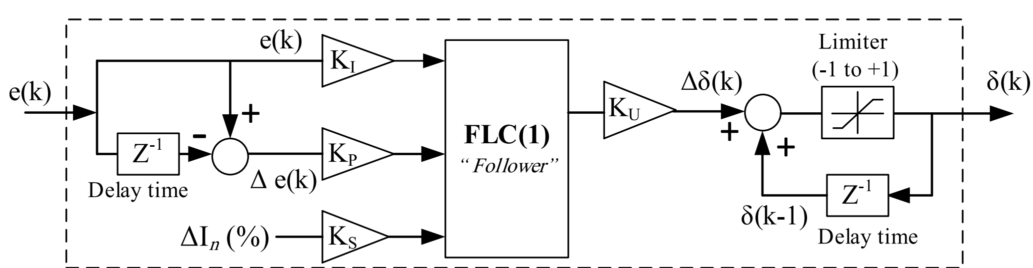

Fig. 6 Schematic block diagram of FLC (1-*Follower*) for the follower buses

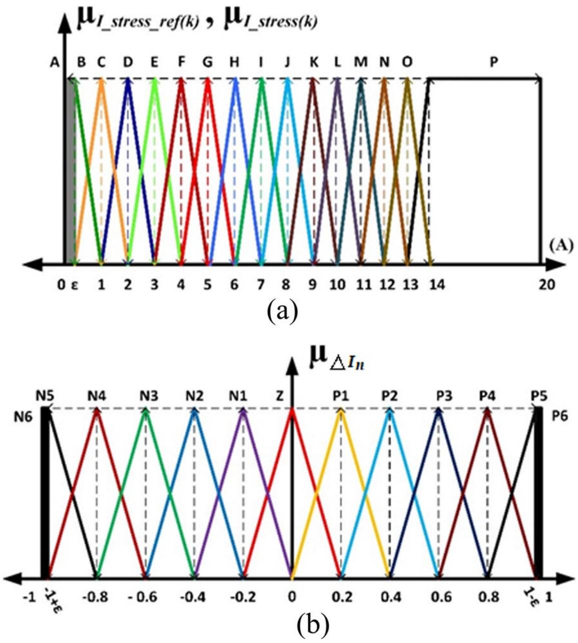

Fig. 8 Membership functions of FLC (2): **a** for the two inputs; **b** for the output

when the first input belongs to {A} while the second input is {B}. It indicates that the reference battery stress current is small and decreases so the output membership function is {N2}. The second exception happens when the second input is {P}, which indicates that the battery stress current has an extreme value which should be decreased immediately as illustrated in Fig. 18 in the Appendix.

3.3 Third controller, FLC (3)

The injected stress current should be shared based on the available battery capacities in the different phases at the same bus. However, the battery SoC values in the phase at the same bus are likely to be unequal. Consequently, certain batteries are prone to reach their SoC limits quicker than others. The battery sharing coefficients can be expressed as:

$$\lambda_{a,j} + \lambda_{b,j} + \lambda_{c,j} = 1 \tag{9}$$

(at adequate capacities of one or more batteries)

$$\lambda_{a,j} + \lambda_{b,j} + \lambda_{c,j} = 0 \tag{10}$$

(at non-adequate capacities of all batteries)

The remainder SoC (ΔSoC) of the battery at each phase is the subtraction of the SoC from the maximum limit (SoC_{max}), i.e.:

$$\Delta SoC_j = SoC_{\max} - SoC_j \tag{11}$$

Therefore, the battery sharing coefficients can be calculated as:

$$\lambda_{a,j} = \frac{\Delta SoC_{a,j}}{\left(\Delta SoC_{a,j} + \Delta SoC_{b,j} + \Delta SoC_{c,j}\right)} \tag{12}$$

$$\lambda_{b,j} = \frac{\Delta SoC_{b,j}}{\left(\Delta SoC_{a,j} + \Delta SoC_{b,j} + \Delta SoC_{c,j}\right)} \tag{13}$$

$$\lambda_{c,j} = \frac{\Delta SoC_{c,j}}{(\Delta SoC_{a,j} + \Delta SoC_{b,j} + \Delta SoC_{c,j})} \tag{14}$$

FLC (3) is designed to determine the battery sharing coefficients at the *j*th bus based on the battery SoC status in each phase. The permissible range of SoC is from 20 to 90% for Lithium-ion batteries [34].

For easy computation in FLC(3), the minimum SoC (SoC_{min}) is considered as 0% and the maximum SoC (SoC_{max}) is 100%. Thus, the three SOC inputs of FLC(3) in Fig. 3 are the modified SoCs (SoC_{mod}) which is expressed based on the Lithium-ion battery SoC limits, as:

$$SoC_{\text{mod}} = (10/7)SoC_{act} - (200/7) \tag{15}$$

The five input membership functions based on the modified SoC values are illustrated in Fig. 9.

FLC (3) is designed based on Takagi–Sugeno fuzzy inference systems. It is more suitable for this task because of its computational accuracy. Unlike Mamdani fuzzy systems, the output membership function can be a linear equation or a constant [35, 36]. Based on the five input membership functions and (12)-(15), there are 24 output constant values. The output function of FLC (3) is a zero-grade Sugeno fuzzy inference, with constant values, as presented in Table 6 in the Appendix.

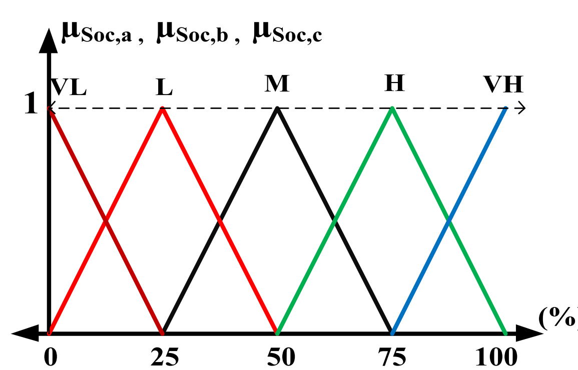

Fig. 9 Five inputs membership functions of FLC (3)

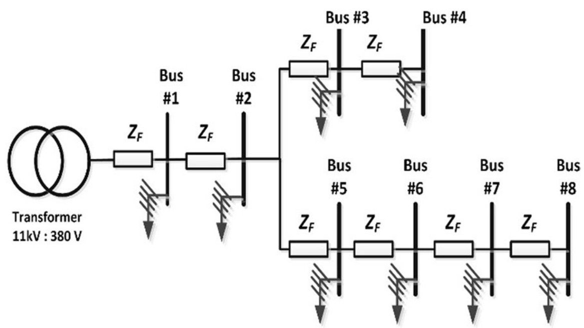

Fig. 10 Schematic diagram of the system under study (radial distribution feeder)

4 System Under Study

The studied system is a three-phase, four-wire radial distribution feeder with eight buses, as shown in Fig. 10. The designed feeder type is four-core copper conductors with a 50 mm^2 cross-sectional area and 0.5 km long. The feeder phase impedance is 0.4940 + j 0.0735 Ω/km. Each bus feeds three single-phase loads with PV and battery systems.

Because of the rapid change of PV generation, four scenarios of PV power values in four sequential periods with fixed load powers (presented in Table 1) are applied in this study.

To examine the proposed controllers during a severe VI, it assumes that all buses have the same active and reactive power, although the power of the phases are different, according to Table 1.

To check the validity of the proposed method with various SoC, one normal case and three extreme cases of SoC of the distributed batteries illustrated in Table 2 are applied. Case 1 is the normal case, in which all batteries have medium SoC values so have sufficient capacities to charge or discharge. Abnormal cases are Cases 2, 3, and 4, in which one or more batteries have reached their maximum limits and there is insufficient SoC for certain batteries.

Table 1 Active and reactive power of the loads and PV generations in four scenarios (kW)

Scenarios	#1	#2	#3	#4	
A	P_{PV}	0.33	0.66	2.00	0
	P_L	2.66	2.66	2.66	2.66
	Q_L	1.33	1.33	1.33	1.33
B	P_{PV}	0.66	1.33	2.00	0
	P_L	2.66	2.66	2.66	2.66
	Q_L	0	0	0	0
C	P_{PV}	1.00	2.00	1.00	1.50
	P_L	1.33	1.33	1.33	1.33
	Q_L	0.43	0.43	0.43	0.43

Table 2 Four cases of SoC (%)

Phase	Case 1	Case 2	Case 3	Case 4
A	50	20	100	0
B	50	70	100	100
C	50	100	0	0

5 Results and Discussions

A sudden change in power flow is the most severe disturbance that occurs in a DN. Thus, the four studied scenarios in Table 1 are applied in sequence to test the effectiveness of the proposed control system. The proposed control system is implemented using MATLAB/SIMULINK. In the following subsections, the following case studies are performed:

(i) determine the VI values in the DN without using any mitigation method;
(ii) apply the proposed control system based on FLC to determine VI and battery currents, and then compare the results with the control system based on PI controllers in [17];
(iii) investigate the effectiveness of the proposed control system in the case of signal loss between buses and noise in the feedback measurements; and
(iv) evaluate the impact of different SoC on battery stress values.

5.1 Base case without control

Without applying the proposed VI mitigation technique, the bus VI values are presented in Fig. 11. The four scenarios are selected to cause four levels of VI to examine the response of the system.

In Scenario #1, the VI values at buses 4, 6, 7, and 8 are 2.17%, 2.26%, 2.49%, and 2.63%, respectively, which exceed the EN 50,160 standard limits. Scenario #2 has more buses that violate the standard limits than Scenario #1 with VI values at buses 3–8 being between 2.32% to 3.65%. The system must shut down when all buses have VI values beneath the standard. Therefore, Scenario #3 which has low VI values is applied between Scenario #2 and Scenario #4 to test the proposed control system validity. Scenario #4 has the highest VI values, where the VI values at buses 2–8 are between 2.07% and 5.51%.

5.2 Applying the proposed control system

By applying the proposed control system, the VI values should be restricted based on the EN 50,160 standard

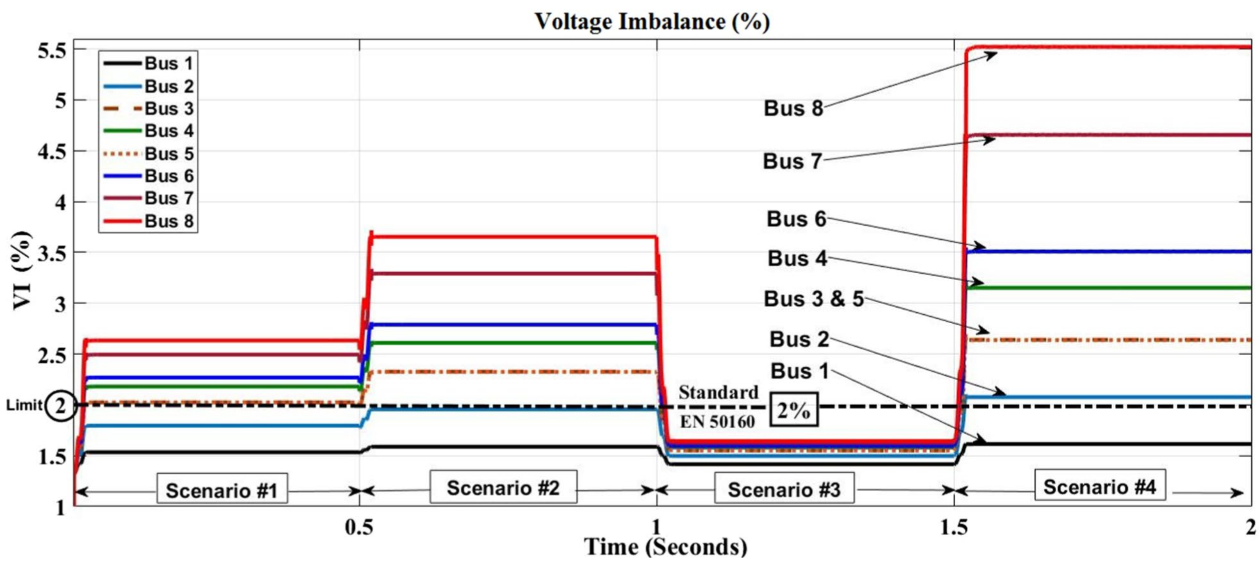

Fig. 11 Bus VI values without applying the VI mitigation control

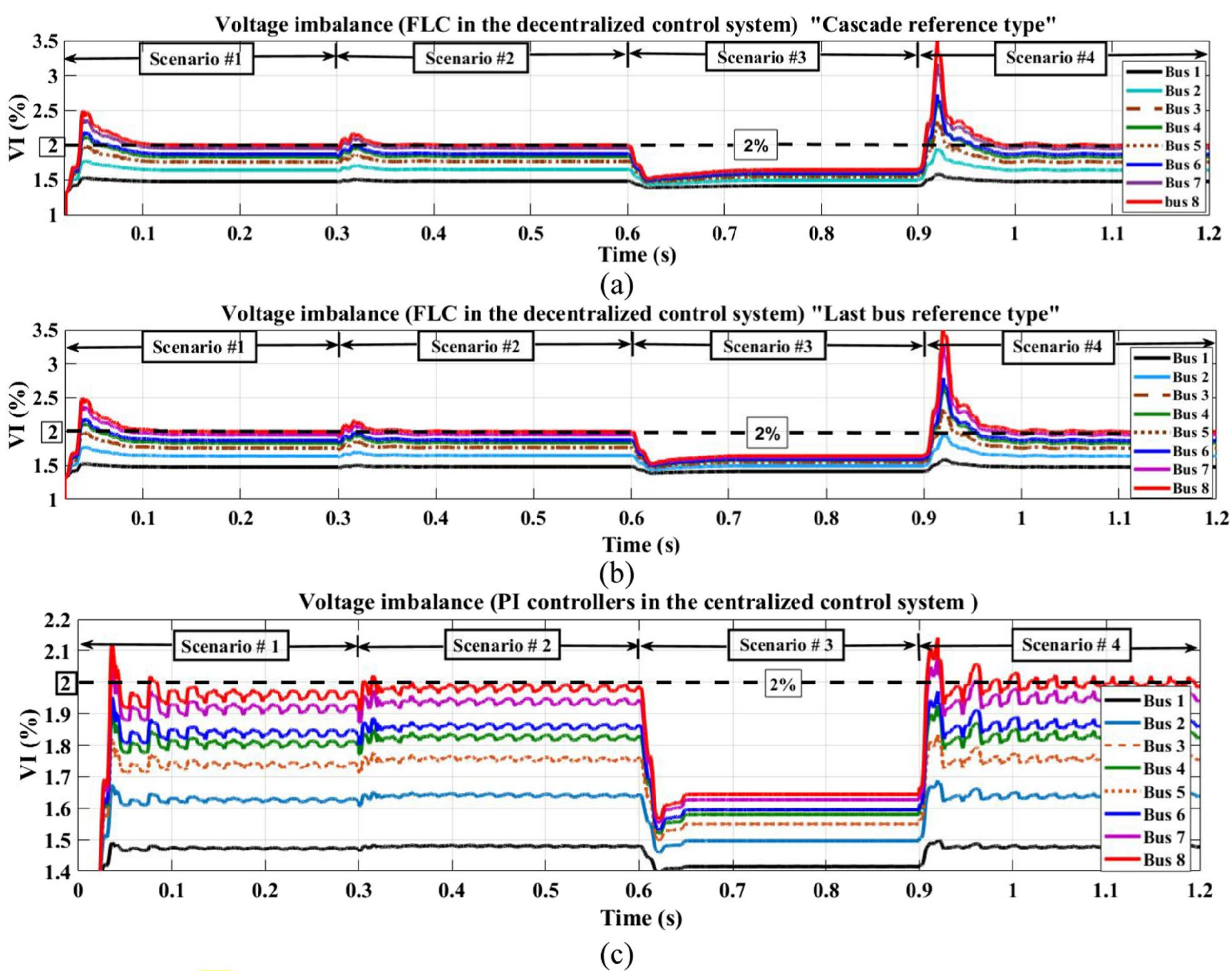

Fig. 12 VI values: **a** cascade bus reference; **b** last bus reference; and **c** conventional PI controllers

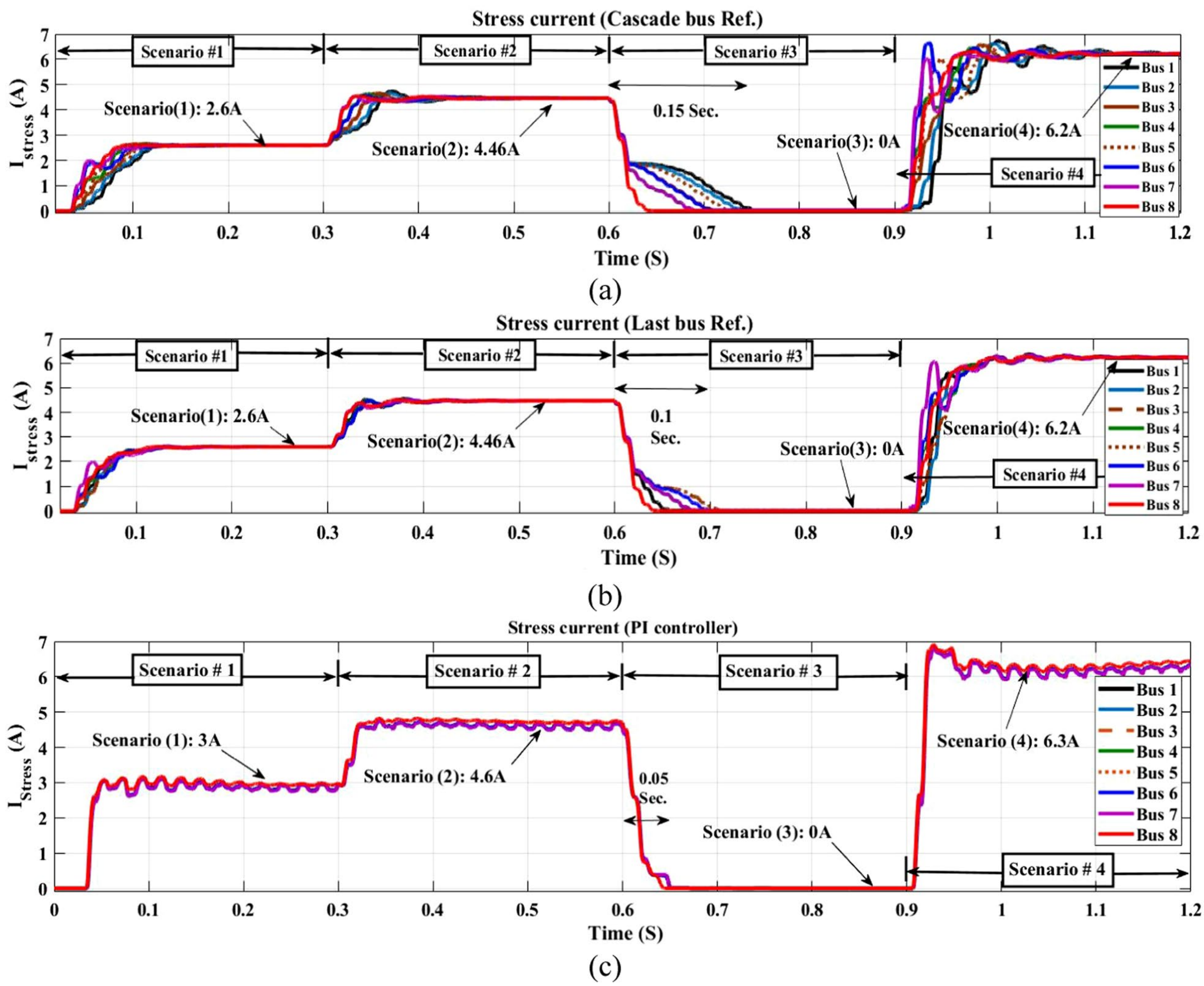

Fig. 13 Stress current: **a** cascade; **b** last bus common references; and **c** conventional PI controllers

with a reference of 2%. As depicted in Fig. 1, two kinds of reference battery stress currents are applied. Figure 12a, b present the VI values by applying the cascade reference and the last bus as a common reference. It assumes that all batteries have the same value as illustrated in Case 1 in Table 2. Thus, the battery sharing coefficients in Case 2 are 0.333, 0.333, and 0.333 for phases *a*, *b*, and *c*, respectively.

As illustrated in Fig. 12a and b, the reference types do not affect the VI results. The largest sudden change occurs when transmitted from the lowest power flow Scenario #3 to the highest power flow Scenario #4. Therefore, it has the highest overshoot value of VI with 3.5%. In contrast, the results of Fig. 12c are from conventional PI controllers in the centralized control scheme in [17], which shows an overshoot of 2.1%. By using the proposed FLC, the steady-state error is zero in all scenarios. The battery stress currents in each bus to mitigate VI in the case of cascade bus reference and last bus common reference are presented in Fig. 13a, b, respectively.

As depicted in Fig. 13a–c, the battery stress currents at all buses have been adjusted to be the same. The steady-state stress current values of FLC are more accurate than conventional PI controllers. Whether using cascade or common references, the corrected stress currents are 2.6 A, 4.46 A, 0 A, and 6.2 A for Scenarios #1–4, respectively. In contrast, the stress currents of the conventional PI-controller are 3 A, 4.6 A, 0 A, and 6.3 A for Scenarios #1–4, respectively. The consequence of these excessive stress currents and VI values are less than 2% in both Scenarios #1 and 2 as shown in

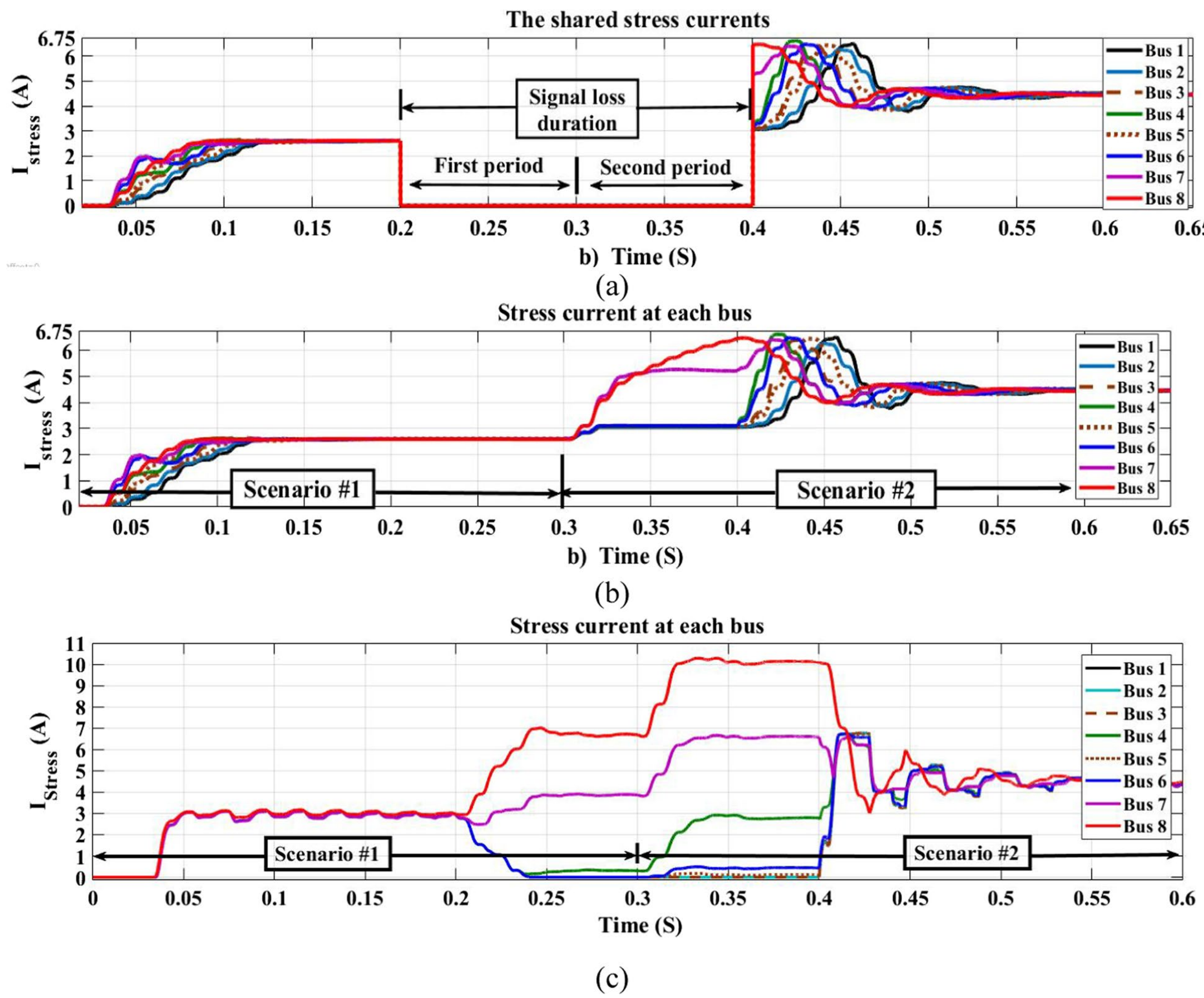

Fig. 14 Impact of signal loss: **a** the shared stress currents; **b** the injected stress currents from the fuzzy controller; and **c** the injected stress currents from conventional PI controllers

Fig. 12c. The merit of the conventional PI controllers is that it has the fastest response.

5.3 Response to signal loss

To test the proposed control system validity, it assumes that all signals among buses have been lost. The signal loss duration occurs at the steady state of Scenario #1 and continues until the power flow is changed in Scenario #2. The signal loss duration is from 0.2 s to 0.4 s, and consists of two periods. The first period occurs in the steady-state of Scenario #1 from 0.2 s to 0.3 s while the second period occurs in the transient time of Scenario #2 from 0.3 s to 0.4 s. The shared battery stress currents among buses and the actual injected battery stress currents in each bus to mitigate VI are presented in Fig. 14a–c.

In case of signal loss in the first period, all shared battery stress currents are zeros but the actual stress currents keep their values until the signal is restored as depicted in Fig. 14b. During the second period from 0.3 s to 0.4 s, the power flow is changed so the buses inject different battery stress currents. Both buses 7 and 8 have the highest VI so they inject the highest battery stress currents of 5.2 A and 6.6 A, respectively. The strength of using FLC is that all buses contribute their stress currents in the case of measurement signal loss. The vulnerability of using PI controllers is the

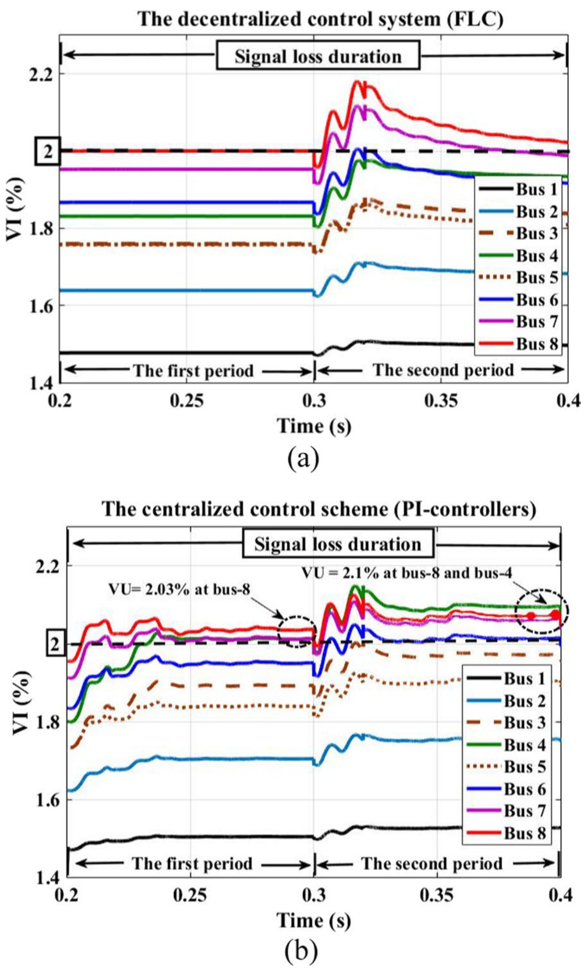

Fig. 15 Bus VI in case of control signal loss: **a** FLC based decentralized control system; and **b** PI controllers based centralized control system

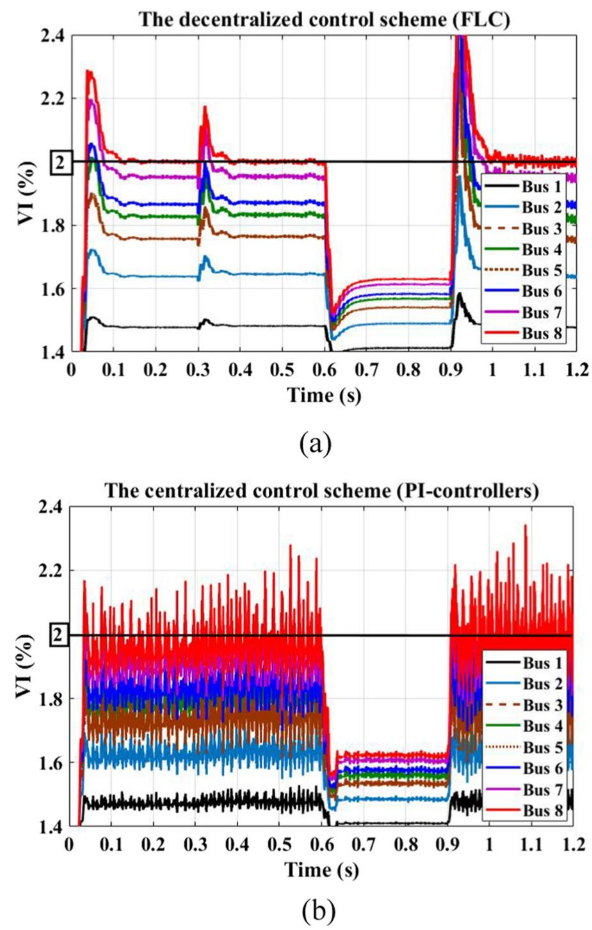

Fig. 16 VI values at applied noise in measurement signals: **a** FLC; and **b** PI controllers

high stress current in the last bus in the DN while stress currents at the beginning of DN are zero as depicted in Fig. 14c. As presented in Fig. 15a, VI is still mitigated in both the steady-state of Scenario #1 and the transient time of Scenario #2. The conventional PI controllers are incapable of mitigating VI under measurement signal loss as shown in Fig. 15b.

5.4 Response to a distorted signal

The last bus is the critical one which has the highest VI. To test the robustness of the proposed system, noise is applied to the measurement signal at bus 8, and the VI results of stress current distortion for both FLC and conventional PI controller are shown in Fig. 16. The maximum noise amplitude that the conventional PI controller can withstand is 20% of the stress currents at bus 8 as depicted in Fig. 16b, while FLC is robust against the same noise as depicted in Fig. 16a.

5.5 Impact of SoC on system response

To test the proposed system validity at different SoC, Cases 2, 3, and 4 in Table 2 are applied. The battery sharing coefficients in Case 2 are 0.731, 0.269, and 0. The coefficients of Case 3 are 0, 0, and 1, and the coefficients of Case 4 are 0.5, 0, and 0.5. Figure 17a presents the battery stress currents in Case 2, while the battery stress currents in Cases 3 and 4 are presented in Figs. 17b and c, respectively.

As presented in Fig. 17b, Case 3 causes the highest battery stress currents in both steady-state and overshoot values. For instance, the highest overshoot of 14 A occurs at Case 3, as presented in Fig. 17b, while Case 1 causes the lowest overshoot of 6.5 A in Fig. 13. Battery

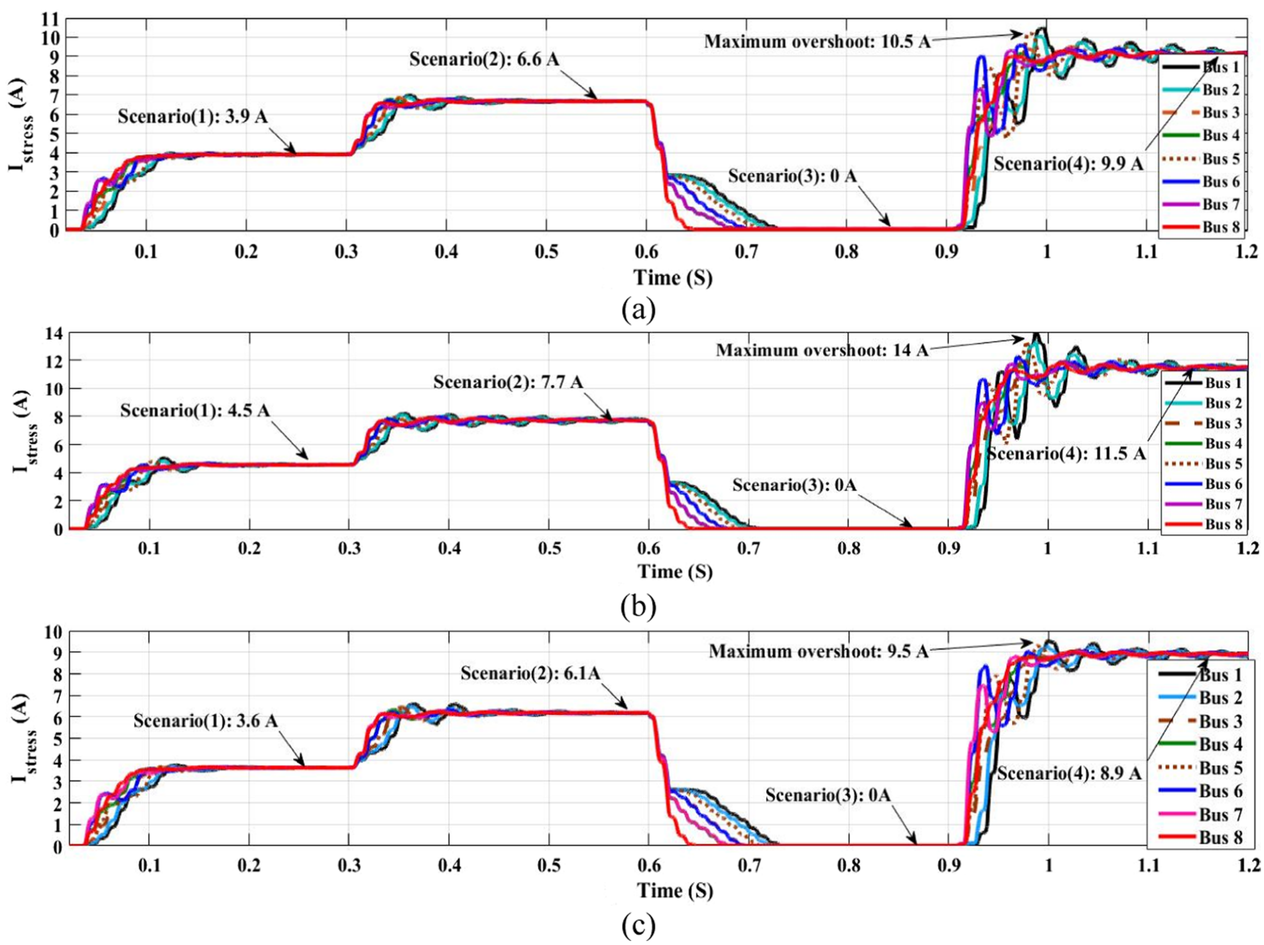

Fig. 17 Battery stress currents at each bus: **a** Case 2; **b** Case 3; and **c** Case 4

stress currents in Cases 2, 3, and 4 increase approximately by 55%, 75%, and 40% respectively in comparison with Case 1. It is concluded that the different SoC values have a significant effect on the steady-state and overshoot values but a minor impact on the transient time.

6 Conclusion

Batteries in domestic rooftop PV systems have the ability to limit high VI in DN. The proposed control scheme is designed based on a decentralized control scheme with minimum communication links. Three FLC are proposed to perform the following tasks, i.e., mitigating the VI values along with the DN buses even in the case of temporary signal loss in communication links, minimizing the steady-state error even with distorted feedback measurements signals, ensuring equal re-share of all battery stress currents in all buses, and re-distributing battery currents at the same bus based on the SoC of each battery. The effectiveness of the proposed control scheme is based on the sudden change of power flows as presented in the four sequential scenarios. The main conclusions of this paper can be summarized as follows.

1. The proposed control system is effective in mitigating VI with zero steady-state error in all scenarios.
2. Both FLC(1-Leader) and FLC(1-Follower) are adequate for mitigating VI in the DN.
3. The proposed control system is immune to both signal measurement loss and noise in the feedback in contrast to the PI-controller [17].
4. The number of communication links of the proposed control system equals the number of buses minus

one, and is one-third of that of a PI controller-based centralized control system.
5. The unified battery current values prevent high stress on batteries at the last bus.
6. The proposed control system has a fast response for mitigating VI values at under 0.1 s.
7. The last common bus reference type is slightly faster than the cascade reference type. However, the cascade reference is more secure.
8. The battery sharing coefficients of FLC (3) prevent both over-charging and over-discharging of batteries. In addition, they decrease battery stress when there is insufficient SoC.

Appendix

See Tables 3, 4, 5 and 6, Fig. 18.

Table 3 Rules of FLC (1- Leader)

Δ*e* / *e*	NL	NS	Z	PS	PL
NL	NL	NL	NL	NS	Z
NS	NL	NS	NS	Z	PS
Z	NL	NS	Z	PS	PL
PS	NS	Z	PS	PS	PL
PL	Z	PS	PL	PL	PL

NL = Negative Lagre, NS = Negative Small, Z = Zero, PS = Positive Small, PL = Positive Lagre

Table 4 Rules of FLC (1-Follower)

e	Δe	ΔI_n	δ	e	Δe	ΔI_n	δ	e	Δe	ΔI_n	δ	e	Δe	ΔI_n	δ	e	Δe	ΔI_n	δ
NL	NL	NL	a	NS	NL	NL	b	Z	NL	NL	c	PS	NL	NL	d	PL	NL	NL	e
NL	NL	NS	b	NS	NL	NS	c	Z	NL	NS	d	PS	NL	NS	e	PL	NL	NS	f
NL	NL	Z	c	NS	NL	Z	d	Z	NL	Z	e	PS	NL	Z	f	PL	NL	Z	g
NL	NL	PS	d	NS	NL	PS	e	Z	NL	PS	f	PS	NL	PS	g	PL	NL	PS	h
NL	NL	PL	e	NS	NL	PL	f	Z	NL	PL	g	PS	NL	PL	h	PL	NL	PL	i
NL	NS	NL	b	NS	NS	NL	c	Z	NS	NL	d	PS	NS	NL	e	PL	NS	NL	f
NL	NS	NS	c	NS	NS	NS	d	Z	NS	NS	e	PS	NS	NS	f	PL	NS	NS	g
NL	NS	Z	d	NS	NS	Z	e	Z	NS	Z	f	PS	NS	Z	g	PL	NS	Z	h
NL	NS	PS	e	NS	NS	PS	f	Z	NS	PS	g	PS	NS	PS	h	PL	NS	PS	i
NL	NS	PL	f	NS	NS	PL	g	Z	NS	PL	h	PS	NS	PL	i	PL	NS	PL	j
NL	Z	NL	c	NS	Z	NL	d	Z	Z	NL	b	PS	Z	NL	f	PL	Z	NL	g
NL	Z	NS	d	NS	Z	NS	e	Z	Z	NS	f	PS	Z	NS	g	PL	Z	NS	h
NL	Z	Z	e	NS	Z	Z	f	Z	Z	Z	g	PS	Z	Z	h	PL	Z	Z	i
NL	Z	PS	f	NS	Z	PS	g	Z	Z	PS	H	PS	Z	PS	i	PL	Z	PS	j
NL	Z	PL	g	NS	Z	PL	h	Z	Z	PL	k	PS	Z	PL	j	PL	Z	PL	k
NL	PS	NL	d	NS	PS	NL	e	Z	PS	NL	f	PS	PS	NL	g	PL	PS	NL	h
NL	PS	NS	e	NS	PS	NS	f	Z	PS	NS	g	PS	PS	NS	h	PL	PS	NS	i
NL	PS	Z	f	NS	PS	Z	g	Z	PS	Z	h	PS	PS	Z	i	PL	PS	Z	j
NL	PS	PS	g	NS	PS	PS	h	Z	PS	PS	i	PS	PS	PS	j	PL	PS	PS	k
NL	PS	PL	h	NS	PS	PL	i	Z	PS	PL	j	PS	PS	PL	k	PL	PS	PL	l
NL	PL	NL	e	NS	PL	NL	f	Z	PL	NL	g	PS	PL	NL	h	PL	PL	NL	i
NL	PL	NS	f	NS	PL	NS	g	Z	PL	NS	h	PS	PL	NS	i	PL	PL	NS	j
NL	PL	Z	g	NS	PL	Z	h	Z	PL	Z	i	PS	PL	Z	j	PL	PL	Z	k
NL	PL	PS	h	NS	PL	PS	i	Z	PL	PS	j	PS	PL	PS	k	PL	PL	PS	l
NL	PL	PL	i	NS	PL	PL	j	Z	PL	PL	k	PS	PL	PL	l	PL	PL	PL	m

Table 5 FLC(1) parameters along the DN

Parameters	Bus-1	Bus-2	Bus-3	Bus-4	Bus-5	Bus-6	Bus-7	Bus-8
K_P	–	1	1	1	1	1	1	1
K_I	–	1	1	1	1	1	1	1
K_S	–	1	1.05	1.2	1.05	1.1	1.2	–
K_U	1.25	1.25	1.25	1.25	1.25	1.25	1.25	0.4

Table 6 The output function of FLC (3)

Crisp	A	B	C	D	E	F	G	H	I	J	K	L
Value	0	0.111	0.125	0.1428	0.1666	0.2	0.222	0.25	0.2727	0.2827	0.3	0.333
Crisp	**M**	**N**	**O**	**P**	**Q**	**R**	**S**	**T**	**U**	**V**	**W**	**X**
Value	0.3636	0.375	0.4	0.4285	0.444	0.5	0.5714	0.6	0.666	0.75	0.8	1

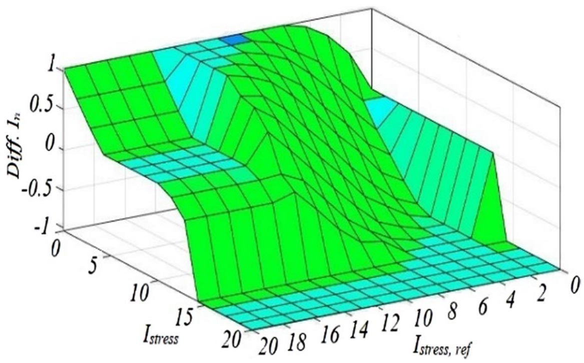

Fig. 18 Surface shape based on rules of FLC (2)

Abbreviations

APC	Active power curtailment
DG	Distributed generators
DN	Distribution network
DR	Demand response
EV	Electric vehicles
FLC	Fuzzy logic controller
HAN	Home area network
IoT	Internet of things
NAN	Neighborhood area networks
NL	Negative large
NS	Negative small
OLTC	On-load tap changer
PL	Positive large
PS	Positive small
PV	Photovoltaic
SoC	State of charge
VI	Voltage imbalance
WAN	Wide area networks
Z	Zero

Acknowledgements
Not applicable.

Author contributions
AMMN: Conceptualization, Software, Writing- Original draft preparation. AAH: Methodology, Reviewing and Editing. MMS: Supervision, Visualization, Reviewing and Editing. AYH: Data curation, Writing, Investigation, Validation. All authors read and approved the final manuscript.

Funding
Not applicable.

Availability of data and materials
All data generated or analyzed during this study are included in this published article.

Declarations

Competing interests
The Authors declare that they have no known competing financial interests or personal relationships that could have appeared to influence the work reported in this paper.

Received: 28 September 2022 Accepted: 14 April 2023
Published online: 14 May 2023

References

1. Kharrazi, A., Sreeram, V., & Mishra, Y. (2020). Assessment techniques of the impact of grid-tied rooftop photovoltaic generation on the power quality of low voltage distribution network: A review. *Renewable and Sustainable Energy Reviews, 120*, 109643. https://doi.org/10.1016/j.rser.2019.109643
2. Nour, A. M. M., Helal, A. A., El-Saadawi, M. M., & Hatata, A. Y. (2021). Voltage violation in four-wire distribution networks integrated with rooftop PV systems. *IET Renewable Power Generation, 14*(13), 2395–2405. https://doi.org/10.1049/iet-rpg.2020.0174
3. Li, R., Wong, P., Wang, K., et al. (2020). Power quality enhancement and engineering application with high permeability distributed photovoltaic access to low-voltage distribution networks in Australia. *Protection and Control of Modern Power Systems, 5*, 18. https://doi.org/10.1186/s41601-020-00163-x
4. Yaghoobi, J., Islam, M., & Mithulananthan, N. (2018). Analytical approach to assess the loadability of unbalanced distribution grid with rooftop PV units. *Applied Energy, 211*, 358–367. https://doi.org/10.1016/j.apenergy.2017.11.030
5. Bandara, W. G. C., Godaliyadda, G. M. R. I., Ekanayake, M. P. B., & Ekanayake, J. B. (2020). Coordinated photovoltaic re-phasing: A novel method to maximize renewable energy integration in low voltage networks by mitigating network unbalances. *Applied Energy, 280*, 1–20. https://doi.org/10.1016/j.apenergy.2020.116022
6. Rahman, M. M., Arefi, A., Shafiullah, G. M., & Hettiwatte, S. (2018). A new approach to voltage management in unbalanced low voltage networks using demand response and OLTC considering consumer preference. *International Journal of Electrical Power & Energy Systems, 99*, 11–27. https://doi.org/10.1016/j.ijepes.2017.12.034
7. Bozalakov, D. V., Laveyne, J., Desmet, J., & Vandevelde, L. (2019). Overvoltage and voltage unbalance mitigation in areas with high penetration of renewable energy resources by using the modified three-phase damping control strategy. *Electric Power Systems Research, 168*, 283–294. https://doi.org/10.1016/j.epsr.2018.12.001
8. Kontis, E. O., Kryonidis, G. C., Nousdilis, A. I., Malamaki, K. N. D., & Papagiannis, G. K. (2019). A two-layer control strategy for voltage regulation of active unbalanced LV distribution networks. *International Journal of Electrical Power & Energy Systems, 111*, 216–230. https://doi.org/10.1016/j.ijepes.2019.04.020
9. Xu, J., Wang, J., Liao, S., Sun, Y., Ke, D., Li, X., Liu, J., Jiang, Y., Wei, C., & Tang, B. (2018). Stochastic multi-objective optimization of photovoltaics integrated three-phase distribution network based on dynamic

scenarios. *Applied Energy, 231*, 985–996. https://doi.org/10.1016/j.apenergy.2018.09.168
10. Zhang, D., Li, J., & Hui, D. (2018). Coordinated control for voltage regulation of distribution network voltage regulation by distributed energy storage systems. *Protection and Control of Modern Power Systems, 3*, 3. https://doi.org/10.1186/s41601-018-0077-1
11. Zeraati, M., Hamedani Golshan, M. E., & Guerrero, J. M. (2018). Distributed control of battery energy storage systems for voltage regulation in distribution networks with high PV penetration. *IEEE Transactions on Smart Grid, 9*(4), 3582–3593. https://doi.org/10.1109/TSG.2016.2636217
12. García-Villalobos, J., Zamora, I., Knezović, K., & Marinelli, M. (2016). Multi-objective optimization control of plug-in electric vehicles in low voltage distribution networks. *Applied Energy, 180*, 155–168. https://doi.org/10.1016/j.apenergy.2016.07.110
13. Farahani, H. F. (2017). Improving voltage unbalance of low-voltage distribution networks using plug-in electric vehicles. *Journal of Cleaner Production, 148*, 336–346. https://doi.org/10.1016/j.jclepro.2017.01.178
14. Carpinelli, G., Mottola, F., Proto, D., & Varilone, P. (2017). Minimizing unbalances in low-voltage microgrids: Optimal scheduling of distributed resources. *Applied Energy, 191*, 170–182. https://doi.org/10.1016/j.apenergy.2017.01.057
15. Camilo, F. M., Castro, R., Almeida, M. E., & Pires, V. F. (2021). Energy management in unbalanced low voltage distribution networks with microgeneration and storage by using a multi-objective optimization algorithm. *Journal of Energy Storage, 33*, 102100. https://doi.org/10.1016/j.est.2020.102100
16. Wong, J., Seng Lim, Y., & Morris, E. (2016). Distributed energy storage systems with an improved fuzzy controller for mitigating voltage unbalance on low-voltage networks. *Journal of Energy Engineering, 142*(1), 04014058. https://doi.org/10.1061/(ASCE)EY.1943-7897.0000260
17. Nour, A. M. M., Helal, A. A., El-Saadawi, M. M., & Hatata, A. Y. (2021). A control scheme for voltage unbalance mitigation in distribution network with rooftop PV systems based on distributed batteries. *International Journal of Electrical Power & Energy Systems, 124*, 106375. https://doi.org/10.1016/j.ijepes.2020.106375
18. Gao, J., Xiao, Y., Liu, J., Liang, W., & Philip Chen, C. L. (2012). A survey of communication/networking in Smart Grids. *Future Generation Computer Systems, 28*(2), 391–404. https://doi.org/10.1016/j.future.2011.04.014
19. Bandeiras, F., Pinheiro, E., Gomes, M., Coelho, P., & Fernandes, J. (2020). Review of the cooperation and operation of microgrid clusters. *Renewable and Sustainable Energy Reviews, 133*, 110311. https://doi.org/10.1016/j.rser.2020.110311
20. Talaat, M., Alsayyari, A. S., Alblawi, A., & Hatata, A. Y. (2020). Hybrid-cloud-based data processing for power system monitoring in smart grids. *Sustainable Cities and Society, 55*, 1–13. https://doi.org/10.1016/j.scs.2020.102049
21. Rachmawati, R., Fauziah, Z., & Safitri, N. (2018). Wireless data communication techniques to coordinate distributed rooftop PVs in unbalanced three-phase feeder. *Telkomnika, 16*(3), 1101–1106. https://doi.org/10.12928/telkomnika.v16i3.7780
22. Almada, J. B., Leão, R. P. S., Sampaio, R. F., & Barroso, G. C. (2016). A centralized and heuristic approach for energy management of an AC microgrid. *Renewable and Sustainable Energy Reviews, 60*, 1396–1404. https://doi.org/10.1016/j.rser.2016.03.002
23. Sun, C.-C., Sebastian-Cardenas, D. J., Hahn, A., & Liu, C.-C. (2021). Intrusion detection for cybersecurity of smart meters. *IEEE Transactions on Smart Grid, 12*(1), 612–622. https://doi.org/10.1109/TSG.2020.3010230
24. Reka, S. S., & Dragicevic, T. (2018). Future effectual role of energy delivery: A comprehensive review of Internet of Things and smart grid. *Renewable and Sustainable Energy Reviews, 91*, 90–108. https://doi.org/10.1016/j.rser.2018.03.089
25. Bhuiyan, E. A., Hossain, M. Z., Muyeen, S. M., Fahim, S. R., Sarker, S. K., & Das, S. K. (2021). Towards next generation virtual power plant: Technology review and frameworks. *Renewable and Sustainable Energy Reviews, 150*, 111358. https://doi.org/10.1016/j.rser.2021.111358
26. Kumar, L. A., Indragandhi, V., Selvamathi, R., Vijayakumar, V., Ravi, L., & Subramaniyaswamy, V. (2021). Design, power quality analysis, and implementation of smart energy meter using internet of things. *Computers & Electrical Engineering, 93*, 107203. https://doi.org/10.1016/j.compeleceng.2021.107203
27. Shrouf, F., & Miragliotta, G. (2015). Energy management based on Internet of Things: Practices and framework for adoption in production management. *Journal of Cleaner Production, 100*, 235–246. https://doi.org/10.1016/j.jclepro.2015.03.055
28. Nour, A. M. M., Hatata, A. Y., Helal, A. A., & EL-Saadawi, M. M. (2018). Rooftop PV systems with distributed batteries for voltage unbalance mitigation in low voltage radial feeders. *Journal of Renewable Sustainable Energy, 10*, 1–20. https://doi.org/10.1063/1.5034000
29. EN 50160. Voltage characteristics of electricity supplied by public distribution systems; May 2005.
30. Cunha, V. C., Freitas, W., Trindade, F. C. L., & Santoso, S. (2020). Automated determination of topology and line parameters in low voltage systems using smart meters measurements. *IEEE Transactions on Smart Grid, 11*(6), 5028–5038. https://doi.org/10.1109/TSG.2020.3004096
31. Kim, H., Choi, H., Kang, H., An, J., Yeom, S., & Hong, T. (2021). A systematic review of the smart energy conservation system: From smart homes to sustainable smart cities. *Renewable and Sustainable Energy Reviews, 140*, 110755. https://doi.org/10.1016/j.rser.2021.110755
32. Benyamina, A., Moulahoum, S., Colak, I., & Bayindir, R. (2017). Design and real-time implementation of adaptive neural-fuzzy inference system controller-based unity single-phase power factor converter. *Electric Power Systems Research, 152*, 357–366. https://doi.org/10.1016/j.epsr.2017.07.025
33. Bilgundi, S. K., Sachin, R., Pradeepa, H., et al. (2022). Grid power quality enhancement using an ANFIS optimized PI controller for DG. *Protection Control of Modern Power Systems, 7*, 3. https://doi.org/10.1186/s41601-022-00225-2
34. Elkazaz, M., Sumner, M., Naghiyev, E., Hua, Z., & Thomas, D. W. P. (2021). Techno-Economic Sizing of a community battery to provide community energy billing and additional ancillary services. *Sustainable Energy, Grids and Networks, 26*, 100439. https://doi.org/10.1016/j.segan.2021.100439
35. Sugeno, M., & Kang, G. T. (1988). Structure identification of fuzzy model. *Fuzzy Sets and Systems, 28*(1), 15–33. https://doi.org/10.1016/0165-0114(88)90113-3
36. Takagi, T., & Sugeno, M. (1985). Fuzzy identification of systems and its applications to modeling and control. *IEEE Transactions on Systems, Man, and Cybernetics.* https://doi.org/10.1109/TSMC.1985.6313399